Nuclear Materials and Energy 12 (2017) 1270–1276

Contents lists available at ScienceDirect

Nuclear Materials and Energy

journal homepage: www.elsevier.com/locate/nme

Measurement of inner wall limiter SOL widths in KSTAR tokamak

J.G. Bak[a,*], R.A. Pitts[b], H.S. Kim[a], H.H. Lee[a], C. Bin[a,d], J.W. Juhn[a], S.H. Hong[a], O.E. Garcia[c], R.A. Kube[c], D.C. Seo[a]

[a] National Fusion Research Institute, Daejeon, Korea
[b] ITER Organization, Route de Vinon-Verdon, CS90 046, 13067 St. Paul Lez Durance Cedex, France
[c] Department of Physics and Technology, UiT The Arctic University of Norway, N-9037 Tromsϕ, Norway
[d] Chineses Academy of Science, Institute of Plasma Physics, Hefei, China

ARTICLE INFO

Article history:
Received 18 July 2016
Revised 15 November 2016
Accepted 1 December 2016
Available online 27 December 2016

Keywords:
KSTAR
Inner wall limiter plasma
SOL width
Narrow feature
Electric probe
IR thermal image

ABSTRACT

Scrape-off layer (SOL) widths λ_q are presented from the KSTAR tokamak using fast reciprocating Langmuir probe assembly (FRLPA) measurements at the outboard mid-plane (OMP) and the infra-Red (IR) thermography at inboard limiter tiles in moderately elongated ($\kappa = 1.45 - 1.55$) L-mode inner wall-limited (IWL) plasmas under experimental conditions such as $B_T = 2.0$ T, $P_{NBI} = 1.4 - 1.5$ MW, line averaged densities $2.5 - 5.1 \times 10^{19}$ m^{-3} and plasma current $I_p = 0.4 - 0.7$ MA. There is clear evidence for a double exponential structure in $q_{||}$(r) from the FRLPA such that, for example at $I_p = 0.6$ MA, a narrow feature, $\lambda_{q,near}$ (=3.5 mm) is found close to the LFCS, followed by a broader width, $\lambda_{q,main}$ (=57.0 mm). Double exponential profiles ($\lambda_{q,near} = 1.5 - 2.8$ mm, $\lambda_{q,main} = 17.0 - 35.0$ mm) can be also observed in the IR heat flux mapped to the OMP throughout the range of I_p investigated. In addition, analysis of SOL turbulence statistics obtained with the FRLPA shows high relative fluctuation levels and positively skewed distributions in electron temperature and ion particle flux across the SOL, with both properties increasing for longer distance from the LCFS, as often previously observed in the tokamaks. Interestingly, the fluctuation character expressed in terms of spectral distributions remains unchanged in passing from the narrow to the broad SOL heat flux channel.

1. Introduction

The issue of limiter scrape-off layer (SOL) heat flux widths has recently become of much greater importance following the realization that the previously simple approximation of a single exponential fall-off from the last closed flux surface (LCFS) assumed in the design of the ITER first wall panel toroidal shaping was invalid and that the SOL in present devices usually exhibits a more complex structure. Double exponential heat flux profiles in the SOL region, a narrow feature (few mm) near the LCFS followed by a broader e-folding length, have now been observed in inner wall-limited (IWL) discharges using fast reciprocating Langmuir probe assemblies (FRLPA) and infra-red (IR) measurements in several tokamaks [1–5]. A multi-machine effort, coordinated by the ITER Organization, has been conducted over the past 3 years, to gather as much data as possible regarding the scaling and physics understanding of this limiter heat flux profile [1,6].

In the KSTAR tokamak, some previous studies have been conducted on the evaluation of the SOL width from FRLPA measurements at the outboard mid-plane (OMP) for outboard wall-limited (OWL) ohmic and L-mode plasmas [7]. Here, radial profiles of electron temperature T_e and ion saturation current density J_{sat} obtained with a triple probe were used to compute the parallel heat flux profile $q_{||}$(r) from which the heat flux width λ_q was extracted. Studies were also performed using the FRLPA of the radial particle flux due to the electrostatic turbulence in the SOL region (with a limited data sampling rate of 0.5 MHz) during H-mode discharges [8]. To complement the multi-device IWL heat flux profile database, these studies have now been extended to IWL plasmas on KSTAR.

In common with the technique employed elsewhere [2–5], measurements of the inboard limiter SOL heat flux profile with a narrow feature near the LCFS on the KSTAR have been obtained using the combination of infra-red (IR) thermography [9], with a tangentially viewing system whose field of view captures the graphite IWL tiles, and the FRLPA providing plasma profiles across the SOL at the OMP. In the IR measurement, $q_{||}$(r) was extracted from

* Corresponding author.
E-mail address: jgbak@nfri.re.kr (J.G. Bak).

http://dx.doi.org/10.1016/j.nme.2016.12.001

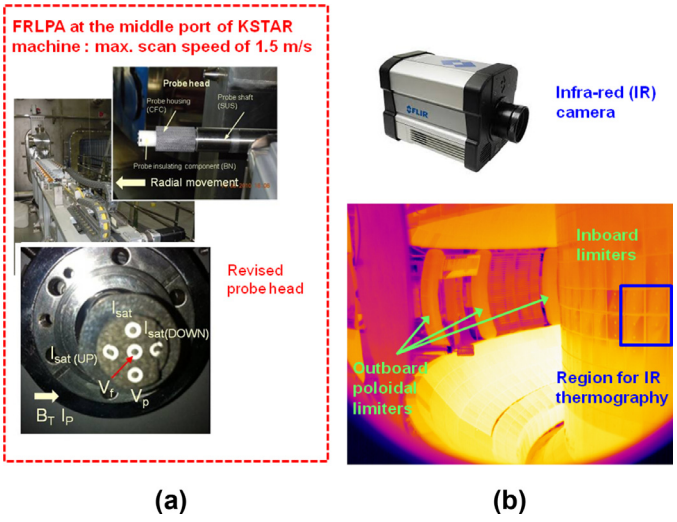

Fig. 1. Diagnostics for evaluating SOL width during IWL plasmas in the KSTAR tokamak: (a) FRLPA together with probe head and (b) IR camera and thermal images of plasma-facing components taken by the IR camera for the system check before plasma experiment (see also Fig. 2 for camera location on the outboard midplane). Here the blue box indicates the region for the IR thermography on the inboard limiter used to extract the heat flux width.

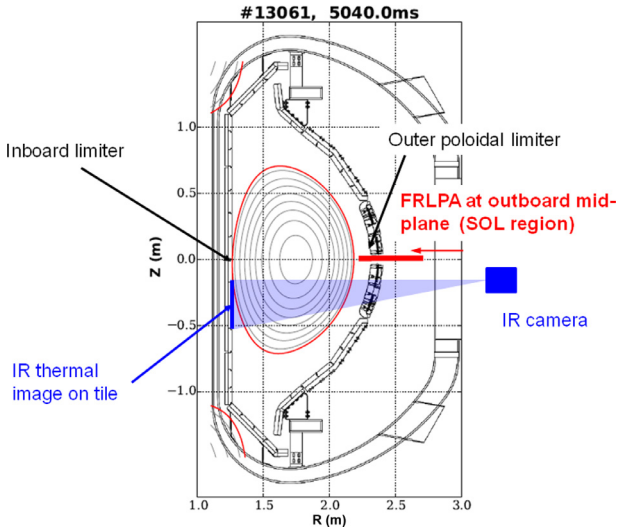

Fig. 2. Real time EFIT reconstructed plasma shape together with the FRLPA for measurement of T_e(r) and J_{sat} (r) at the OMP and the IR camera for measuring the surface temperature at the inboard limiter tile in KSTAR.

thermal analysis of the IR surface temperatures on the IWL tiles, in combination with field line mapping to the OMP. The data acquisition system of the FRLPA was also upgraded for improved turbulence measurements and provided electrostatic fluctuations with 2 MHz sampling rate in both T_e and J_{sat}. In this paper, the diagnostics for evaluating the SOL heat flux profile are briefly described in Section 2, the double-exponential SOL heat flux profiles obtained from the FRLPA and IR measurements in the IWL plasmas are presented in Section 3, and the preliminary results from analysis of electrostatic fluctuations in the SOL profiles at the OMP are mentioned in Section 4. More extensive analysis of the statistics of particle flux density turbulence, obtained in a dedicated diverted L-mode density scan, is found in Ref. [10]. Finally, a summary is given in Section 5.

2. Description of diagnostics for SOL heat flux profile

Fig. 1(a) shows the FRLPA together with a revised probe head (compared to the previous probe head described in [11]) for radial profile measurements at the OMP in the KSTAR. A total of five probe tips are installed in the FRLPA probe head; three poloidally and two toroidally separated tips for the triple and Mach probe measurements, respectively. Here, the elapsed distance of the FRLPA is measured by the photoelectric sensor [11] for evaluating Δr_{sep}, which is also checked with the position of the last closed flux surface (LCFS) reconstructed from the EFIT code. The FRLPA data acquisition sampling rate has been upgraded up to 2.0 MHz to improve electrostatic turbulence measurements. Further details of the FRLPA system may be found in [11].

Fig. 1(b) shows an IR camera (FLIR / ThermoVision SC6000HS) used for measuring surface temperature on the graphite tiles used for inboard limiters and outer poloidal limiters during plasma discharges. The IR camera is a wide field, tangentially viewing system whose field of view (FOV) captures the graphite tiles loaded during both IWL and OWL discharges. The IR camera provides a 2D thermal image of 640×512 pixels corresponding to $\sim 1670 \times 1540\,mm^2$ and a full frame rate of $1-125$ Hz with noise equivalent temperature difference (NETD) ≤ 25 mK. The spatial resolution of the IR images is in the range of $2.6-3.0$ mm/pixel. The region of interest covering three inner wall tiles which have been used for the heat flux density analysis presented here are marked inside the rectangular box in Fig. 1(b). Thus, a thermal image of area only $94 \times 390\,mm^2$ corresponding to 35×135 pixel inside the full FOV was used to extract the SOL heat flux profiles for comparing with those measured by the FRLPA.

3. SOL heat flux profile in IWL plasmas

The double-exponential SOL parallel heat flux $q_{||}$(r), with a narrow feature $\lambda_{q,near}$ near the LCFS and a broader e-folding length $\lambda_{q,main}$ in the main SOL region, can be expressed [1] as

$$\begin{aligned} q_{\parallel}(r) &= q_{\parallel,near}(r) + q_{\parallel,main}(r) \\ &= q_{\parallel,near}(0)e^{\left(\frac{-\Delta r_{sep}}{\lambda_{q,near}}\right)} + q_{\parallel,main}(0)e^{\left(\frac{-\Delta r_{sep}}{\lambda_{q,main}}\right)}, \end{aligned} \tag{1}$$

where Δr_{sep} is the radial distance from the LCFS, and $q_{||,near}$(r) and $q_{||,main}$(r) are the heat fluxes near the LCFS and in the main SOL region, respectively and $q_{||,near}(0)$ and $q_{||,main}(0)$ are the heat fluxes extrapolated to the LCFS. Using the relationship $R_q = q_{||,near}(0)/q_{||,main}(0)$, together with 0D power balance at the LCFS [1], the parallel heat fluxes $q_{||}(0)$ and $q_{||,main}(0)$ at the LCFS may be written;

$$\begin{aligned} q_{\parallel}(0) &= q_{\parallel,main}(0)(1+R_q), \\ q_{\parallel,main}(0) &= \frac{P_{SOL}}{4\pi R_{OMP}\left(R_q \cdot \lambda_{q,near} + \lambda_{q,main}\right)(B_\theta/B_{total})_{OMP}} \end{aligned} \tag{2}$$

where R_{OMP}, B_θ and B_{total} are the major radius, poloidal and total magnetic fields, respectively at the OMP and the power to the SOL, $P_{SOL} = P_{heating} - dW_{TOT}/dt - P_{rad}$ where $P_{heating}$, W_{TOT} and P_{rad} are the total heating power (ohmic + auxiliary heating), the stored energy and the radiative power, respectively.

Experiments for the SOL width measurements were performed in moderately elongated ($\kappa = 1.47-1.55$) deuterium L-mode IWL plasmas as shown in Fig. 2. The experimental conditions were as follows; $B_T = 2.0$ T; plasma current, $I_p = 0.4-0.7$ MA; line averaged density, $n_e = 2.5-5.1 \times 10^{19}\,m^{-3}$; neutral beam (NB) power, $P_{NB} = 1.4-1.5$ MW; ohmic power, $P_{OH} = 0.16-0.31$ MW; safety factor at the 95% flux surface, $q_{95} = 3.2-5.7$. The major and minor radii were $R_0 = 1.75-1.79$ m and $a = 0.46-0.47$ m, respectively.

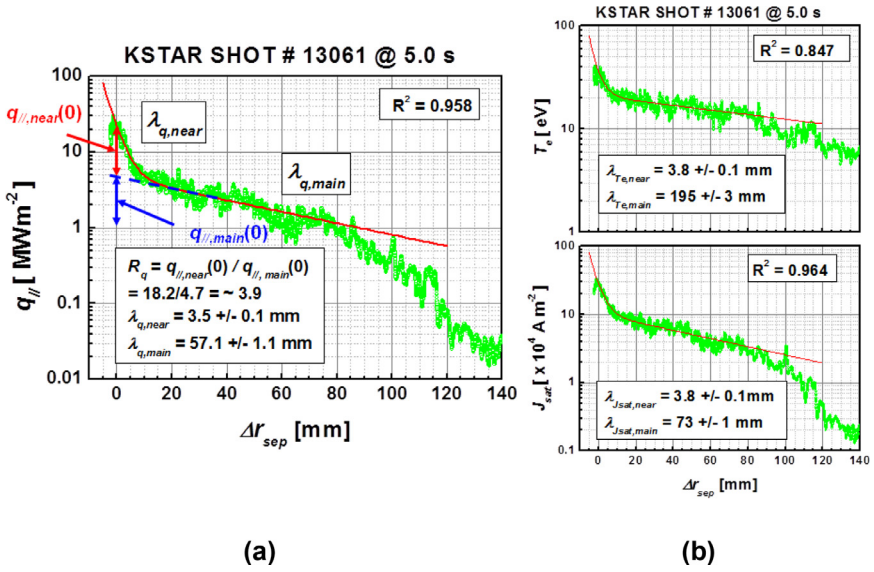

Fig. 3. Radial SOL profiles from the FRLPA measurement at the OMP in an IWL plasma: (a) parallel heat flux $q_{||}$(r), and (b) the electron temperature T_e(r) and ion saturation current density J_{sat}(r) profiles used to evaluate $q_{||}$(r).

3.1. FRLPA measurement at the OMP

The radial profiles of $q_{||}$(r) were evaluated from the T_e(r) and J_{sat}(r) profiles obtained from the FRLPA measurements in the standard way using $q_{||}(r) = \gamma T_e(r) \cdot J_{sat}$ (r)/$Z_{eff} \cdot e$ where γ is the heat transmission coefficient assumed as $\gamma = 7$ ($T_e \approx T_i$). The effective charge Z_{eff} was evaluated from visible bremsstrahlung measurements and $Z_{eff} = 3$ was used here. Only radial profiles obtained during the inward FRLPA movements were used to evaluate the SOL width due to hysteresis observed in the measured profiles during the outward motion.

There is a clear evidence of a double exponential decay structure in $q_{||}$(r) from the FRLPA measurement such that a narrow feature, $\lambda_{q,near}$ is found close to the LFCS, followed by a broader width, $\lambda_{q,main}$ during an IWL plasma as shown in Fig. 3(a). The fitted double exponential profile gives $\lambda_{q,near} = 3.5$ mm and $\lambda_{q,main} = 57.1$ mm ($R^2 = 0.958$) from which $R_q \sim 3.9$ and $q_{||}(0) = 22.9$ MW m^{-2} are also obtained. The neutral beam (NB) power P_{NB} was the major contributor to $P_{heating}$ in these discharges. Unfortunately, no total radiative power measurements were available during these discharges. The value of $q_{||}(0)$ is thus estimated assuming $P_{rad} = 0.16 \cdot P_{heating}$ ($P_{SOL} = 1.3$ MW) from a radiative power measurement ($P_{rad} = \sim 0.5$ MW for $P_{heating} = 3.2$ MW) obtained from foil bolometer cameras in a previous L-mode plasma (shot 11,398). The value of $q_{||}(0) = 23.9$ MW m^{-2} is then obtained from Eq. (2) using the measured $\lambda_{q,near}$, $\lambda_{q,main}$ and R_q. The $q_{||}(0)$ from the FRLPA measurement matches well with the simple power balance estimate. As shown in Fig. 3(b), at $I_p = 0.6$ MA double-exponentially decaying profiles are also clearly observed in both T_e(r) and J_{sat} (r) with $\lambda_{Te,near} = \sim 3.8$ mm, $\lambda_{Jsat,near} = \sim 3.8$ mm and $\lambda_{Te,main} = \sim 195.0$ mm, $\lambda_{Jsat,main} = \sim 73.0$ mm. For discharges with $I_p = 0.4$ and 0.7 MA, only main SOL widths were obtained with the FRLPA measurements (see Fig. 7(b)), since, unfortunately, it turned out that the FRLPA did not reach the near-SOL region in these discharges.

3.2. IR thermography at inboard limiter tile

Fig. 4(a) shows the wide angle IR thermal images (including the inboard central column and the outer poloidal limiter tiles) during the inner wall limiter (IWL) plasma discharge at $I_p = 0.6$ MA. The perpendicular heat flux density $q_\perp$ on the inboard limiter tiles is evaluated using a heat flux reconstruction code (NANTHELOT) solving the heat diffusion equation with the measured tile surface temperature by applying the finite volume method [12]. The code can provide 1D, 2D and 3D profiles of heat flux. There are two particular bright regions on the inboard tiles in the IWL discharges seen in Fig. 4(a), which are almost certainly due to the tile misalignments with respect to the magnetic field lines. The thermal image on the misaligned tile is used to obtain better heat flux profiles. Fig. 4(b) shows the 2D distribution of $q_\perp$ evaluated using NANTHELOT for one poloidal set of tiles with good heat flux data. Here, the pixel numbers on the x and y axes correspond to toroidal angle and vertical position, respectively. Pixel numbers 579 and 565 on the x-axis correspond to toroidal angles of 202.7° and 204.6°, respectively.

In order to evaluate the parallel heat flux from $q_\perp$, the incidence angle θ_{inc} between the direction tangent to the limiter surface and the magnetic field line ($\theta_{inc} = \sin^{-1}$ (B_θ /B_{tot}) $+ \alpha + \delta\theta_{tilt}$) was obtained by using results from magnetic equilibrium reconstruction with the real time EFIT code. Here, B_{tot} is total magnetic field and B_θ is the poloidal magnetic field expressed as $B_\theta = B_R$ using only radial component B_R of the poloidal field. In addition, α and $\delta\theta_{tilt}$ are other angles which may be caused by the tile geometry and the tile misalignment, respectively. Given that no measurement of the potential tile misalignment is available, α and $\delta\theta_{tilt}$ are determined purely geometrically, accounting for the flat tile geometry (width 12 cm) and the expected tilt angle due to the tile misalignment (up to ±0.5 mm) in the toroidal direction, respectively. The value of α at the edge of the tile is estimated as ~2.7° and the maximum value of $\delta\theta_{tilt}$ is ±0.48°. Thus, the range of θ_{inc} used for evaluation of parallel heat flux is $(2.7 - 3.8)° \pm 0.48°$ as shown in Fig. 5(a) because the IR thermal image appears near the edge tile as seen in Fig. 4(a), and there is a linear relationship between Z and θ_{inc} in the range of the IR thermal image (-41 cm $< Z < -4$ cm). This range is nearly equal to the vertical length covered by three lower inboard limiter tiles (vertical length of one limiter tile is ~14 cm).

Each vertical point of thermal images on the tile surface in the inboard limiter is mapped to the radial coordinate at the OMP by using results from the magnetic equilibrium reconstruction data. As seen in Fig. 5(b), the vertical range of ~37 cm maps to an OMP radial range of ~34 mm. It should be noted that the relatively high values of θ_{inc} mean that the IR power flux density is unlikely to be influenced by cross-field power deposition ("funneling" effect) known to be a factor at very glancing angles of incidence [2,5].

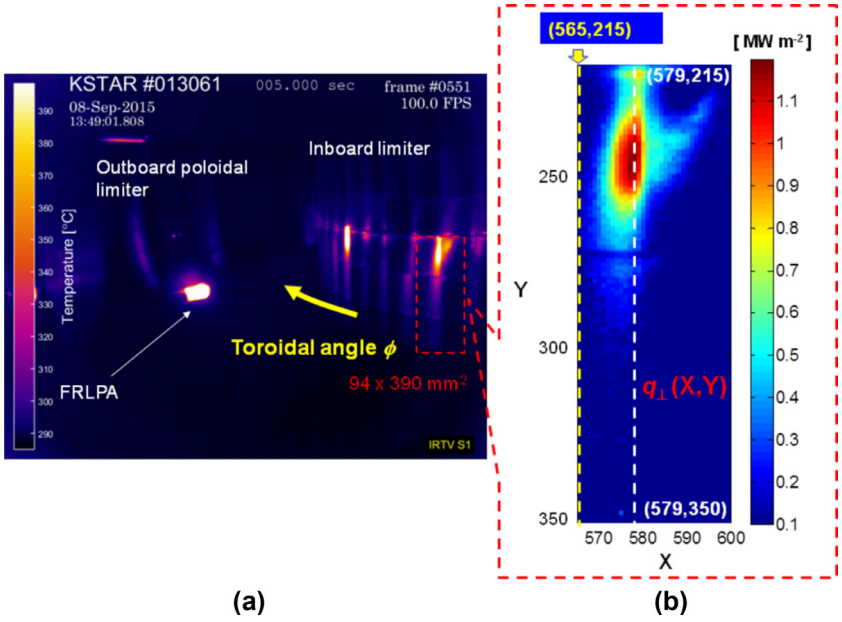

Fig. 4. (a) Thermal wide angle images acquired with the IR camera located at the midplane port 'D' and (b) 2D heat flux density on the inboard limiter tiles obtained from the IR thermal image using the NANTHELOT code. Here, thermal image of area $94 \times 390\,mm^2$ corresponds to 35×135 pixels. The pixel number of 565 for the evaluation of the heat flux due to a radiated power as a background.

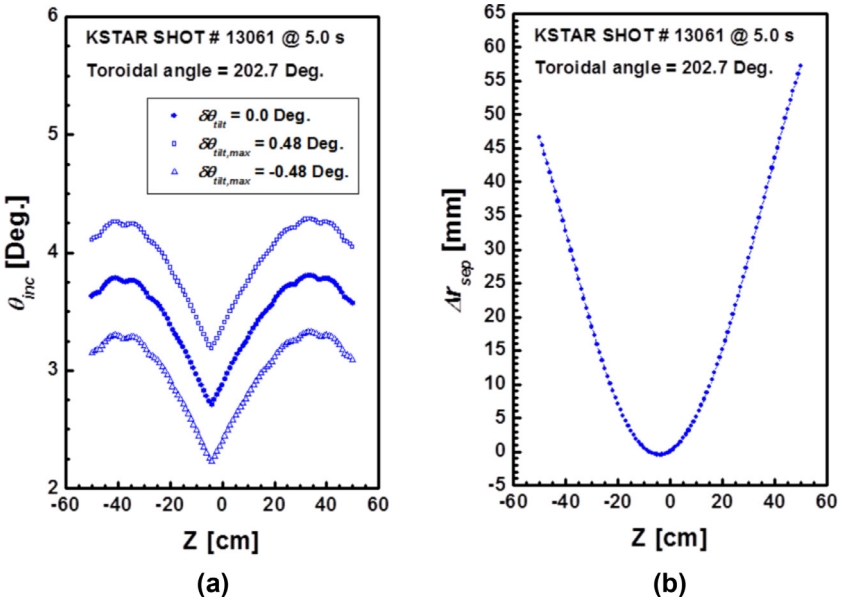

Fig. 5. (a) Incidence angle θ_{inc} between the limiter surface and magnetic field B versus vertical position Z for a toroidal angle $\phi = 202.7°$ at the inner limiter tiles, and (b) radial distance from the LCFS mapped from Z using the poloidal flux from the real time EFIT code.

At a toroidal angle of 202.7°, Fig. 6(a) shows the profile of $q_\perp$ (Z) on the inboard tiles. The maximum value of $q_\perp$ is ~1.1 MW m^{-2}. Here, the influence of a radiated power is also investigated by using the profile extracted from the image at the angle of 204.6°, and there is no clear variation in the profile with the maximum value of ~0.1 MW m^{-2} as shown in Fig. 6(a). Thus, the radiated power as a background was not included in the evaluation of the parallel heat flux profile. The corresponding mapped radial parallel heat flux profile $q_{||}(r)$ evaluated according to $q_{||}(r) = q_\perp(r)/\sin\theta_{inc}$ is shown in Fig. 6(b), demonstrating the familiar double-exponential parallel SOL heat flux profile seen with the FRLPA in Fig. 3 in the same discharge (13,061). A narrow SOL width near the LCFS ($\lambda_{q,near} = 1.5$ mm) and a broader width ($\lambda_{q,main} = \sim 21.0$ mm) are obtained from a double exponential fit ($R^2 = 0.977$). Here, the SOL width was evaluated from the IR heat flux profile used the data averaged over ten profiles in the toroidal angle range of 202.7 – 203.9°.

The value of R_q extracted from the fit is ~9.0, which is about a factor 2 higher than that derived from the FRLPA profile for the same discharge. Regarding $q_{||}(0)$, the value obtained from the IR profile is 16.0 MW m^{-2}, compared with 22.9 MW m^{-2} from the FRLPA, which can be considered satisfactory agreement given the use of a standard value for the sheath heat transmission factor in deriving $q_{||}(r)$. In addition, the values in $q_{||}(r)$ are slightly changed

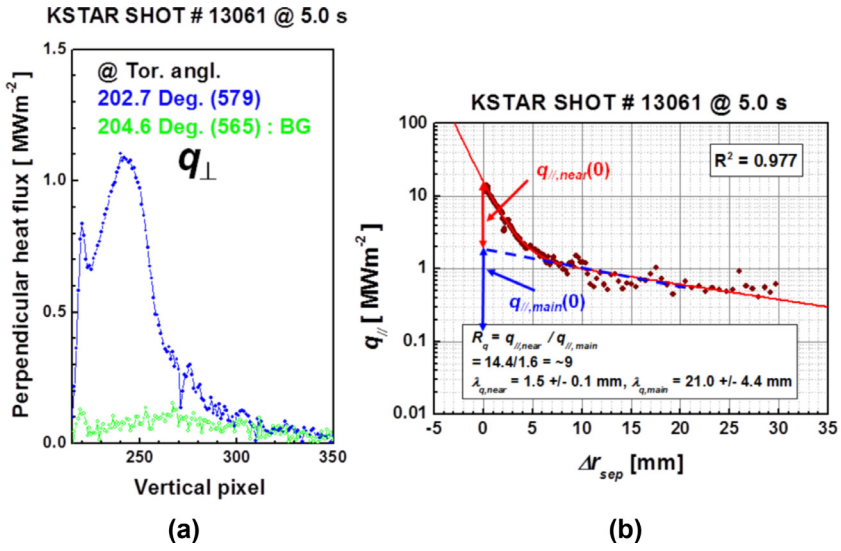

Fig. 6. (a) Perpendicular heat flux profiles extracted from the IR measurements seen Fig. 4(b) at toroidal angles of 202.7° and 204.6°, and (b) the parallel heat flux (from the averaged data of the ten profiles) mapped to the OMP for $\delta\theta_{tilt} = 0°$. Here, one vertical pixel corresponds to 2.6 – 3.0 mm/pixel in (a).

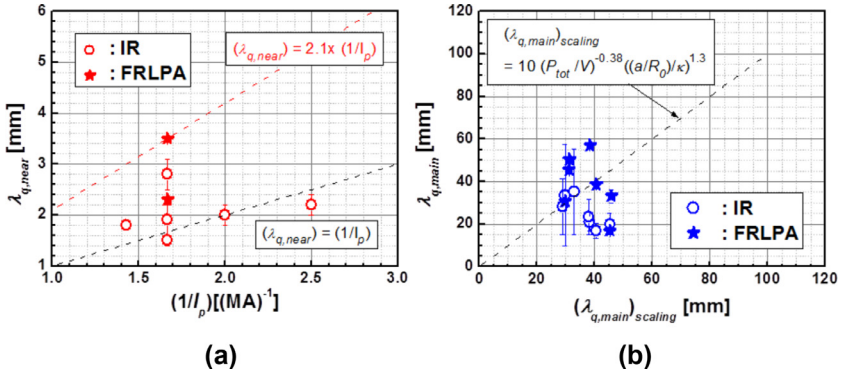

Fig. 7. SOL heat flux widths from FRLPA and IR measurements: (a) $\lambda_{q,near}$ versus 1/ I_p and (b) $\lambda_{q,main}$ versus the recent multi-machine scaling for the main SOL limiter heat flux width using Eq. (3).

Table 1
The values of $q_{||}(0)$ and SOL widths from the evaluation of $q_{||}(r)$ by including $\delta\theta_{tilt}$ for shot 13,061 shown in Fig. 6(b).

$\delta\theta_{tilt}$ [°]	$q_{||}(0)$ [MW m^{-2}]	$\lambda_{q,near}$ [mm]	$\lambda_{q,main}$ [mm]
0	16.0	1.5	21.0
0.48	13.6	1.5	21.8
−0.48	18.9	1.5	20.9

as given in Table 1 when $\delta\theta_{tilt}$ is included in the evaluation of $q_{||}(r)$. Here, the change in the SOL width due to the tile misalignment is expected as less than 4%.

3.3. Comparison between SOL widths from FRLPA and IR measurements

From the FRLPA at $I_p = 0.6$ MA, $\lambda_{q,near}$ and $\lambda_{q,main}$ were 2.3 – 3.5 mm and 39.0 – 57.0 mm, respectively, $R_q = \sim 3.9$ and $\lambda_{q,main} = 17.0 – 57.0$ mm for other values of I_p. From the IR thermography, for which data is available for the whole SOL profile for the range of I_p studied, $\lambda_{q,near} = 1.5 – 2.8$ mm, $\lambda_{q,main} = 17.0 – 35.0$ mm and $R_q = 3.2 – 9.2$ in the range of 0.4 – 0.7 MA. The value of $\lambda_{q,near}$ is $\sim 0.1\lambda_{q,main}$. The data for $\lambda_{q,near}$ and $\lambda_{q,main}$ are gathered in Fig. 7(a) and (b), respectively.

Here, they are plotted against $1/I_p$ for $\lambda_{q,near}$, and for $\lambda_{q,main}$ against the recently published multi-machine scaling [6]:

$$\lambda_{q,main} = 10(P_{tot}/V)^{-0.38}((a/R_0)/\kappa)^{1.3} \quad (3)$$

where P_{tot}/V is the total heating power per plasma volume in unit of [Wm^{-3}].

The data for $\lambda_{q,near}$ come mostly from the IR measurements as described above (the FRLPA did not reciprocate close enough to the LCFS for many of the discharges in the plasma current scan). They show the evidence for decrease of $\lambda_{q,near}$ with increasing I_p (or B_θ), but there are insufficient data for good statistics. In general, the measured values of $\lambda_{q,near}$ in the range 2 – 4 mm from these elongated KSTAR IWL plasmas are comparable to those obtained from the five tokamaks contributing to the study in [1] (see Table 1 in that paper). For the main SOL widths, the data are again scattered and fall generally within a factor 2 of the multi-machine scaling. This is in fact also the case for the majority of the data from other tokamaks constituting the scaling database. Such scatter is not unusual when considering the very many uncertainties which arise when using Langmuir probes in particular to measure SOL profiles.

4. Analysis of electrostatic fluctuation at the SOL

As described in Section 2, the FRLPA was also equipped for turbulence measurements with 2 MHz acquisition rate and provided fluctuations in both the radial profiles of T_e and J_{sat} (see

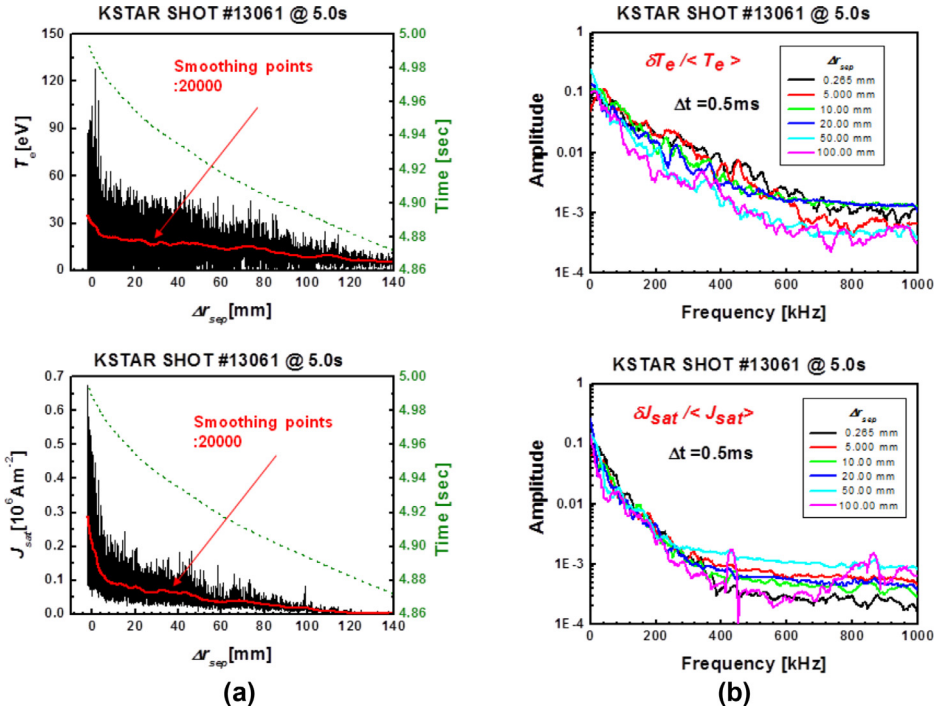

Fig. 8. (a) Radial profiles of T_e and J_{sat} together with elapsed time versus radial distance from the LCFS (green dotted curves), and (b) FFT spectrograms of $\delta T_e/<T_e>$ and $\delta J_{sat}/<J_{sat}>$ at six different radial locations (1000 data elements for each location). Data are obtained from the FRLPA measurement during the same L-mode IWL plasmas used to study the SOL heat flux profiles described earlier. Further clear evidence for the double-exponential profile can be seen in the smoothed red curves in (a) for both T_e and J_{sat}.

Fig. 8(a)) during the experiments designed to study the SOL heat flux profiles. Fig. 8(b) shows FFT spectrograms at a variety of radial positions in the OMP SOL for shot 13,061 at $I_p = 0.6$ MA. Each spectrogram is obtained using 1000 datapoints (0.5 ms) corresponding to a sub-millimeter radial distance (0.2 – 0.9 mm), such that the FRLPA may be considered effectively at rest for duration of the sampling. This radial distance is also comparable to the radial extent (0.8 mm) of the probe tip. From the region near the LCFS (0.3 mm $< \Delta r_{sep} <$ 10.0 mm) to the main SOL region ($\Delta r_{sep} >$ 20 mm), there is evidently no clear difference between the spectrograms in the near and main SOL regions.

For some basic studies of fluctuation statistics following the approach in [10], the data time series from the probe reciprocations are divided into sub-records of 5 ms duration corresponding to ~0.5 cm movement of the FRLPA, giving 10^4 data elements per bin for the T_e and I_{sat} profiles. This number of data elements has been found as the best compromise between spatial resolution and convergence of estimators for the lowest order statistical moments. By using these sub-records, the sample mean, standard deviation, skewness and flatness moments of T_e and I_{sat} may be calculated as shown in Fig. 9. The skewness and flatness moments for I_{sat} increase up to 2.5 and 10, respectively, with increasing radial distance from the LCFS. This is similar to previous measurements of this type obtained in other tokamaks [13–15] – high relative fluctuation levels with strongly positive-skewed and flattened particle flux density probability distribution functions. Interestingly, although the relative fluctuation levels of T_e and I_{sat} (see Fig. 9(a)) are similar through the SOL, the skewness and flatness of the T_e fluctuations is significantly lower than for the ion flux and remains constant across the SOL width.

5. Summary

Double-exponential SOL heat flux profiles with a narrow feature ($\lambda_{q,near} = 2 - 4$ mm) followed by a broader width ($\lambda_{q,main} = 17.0 -$ 57.0 mm) are clearly observed in KSTAR inner wall limited, L-mode plasmas from both fast reciprocating Langmuir probe measurements in the outer midplane SOL and IR measurements of surface heat flux density on inner wall midplane limiter tiles. In general, for the restricted database available, the heat flux widths measured by the probe are higher than those extracted from the IR measurements. These KSTAR results are important in the sense that most previous experiments of this type on other tokamaks have not detected the narrow feature in both probe and IR measurements in the same discharge.

There are insufficient data points and the scatter is significant within the 0.4 – 0.7 MA current scan performed in these experiments to deduce any clear scalings. On the basis of the measurements of near-SOL width from the IR camera, there is a trend for $\lambda_{q,near}$ to scale approximately with $1/I_p$, as seen from compilations of such measurements from other tokamaks (see e.g. Ref. [16]). In general, the KSTAR values of $\lambda_{q,near}$ are comparable to those from other tokamaks. For the main SOL, the KSTAR data are within a factor of 2 of the recently published multi-machine scaling in [6]. Values of the parameter R_q, important for the ITER inboard wall shaping design are also found on KSTAR to be comparable to those measured elsewhere [1], adding further confirmation that this narrow feature is universal and should be expected to be present on ITER.

Some basic analysis of turbulence statistics in T_e and I_{sat} across the SOL has been performed to investigate the properties of the electrostatic fluctuations in the two regions with narrow and broader SOL widths. This analysis complements the more comprehensive study from the KSTAR probe data in [10]. High relative fluctuation levels and positively skewed distributions are found in both T_e and I_{sat} across the SOL, with both properties increasing with increasing distance from the LCFS for the ion flux, as often observed in the tokamak SOL. On KSTAR, however, the skewness and flatness moments in T_e are found to be much lower than those in particle flux. No clear difference is seen in basic spectral

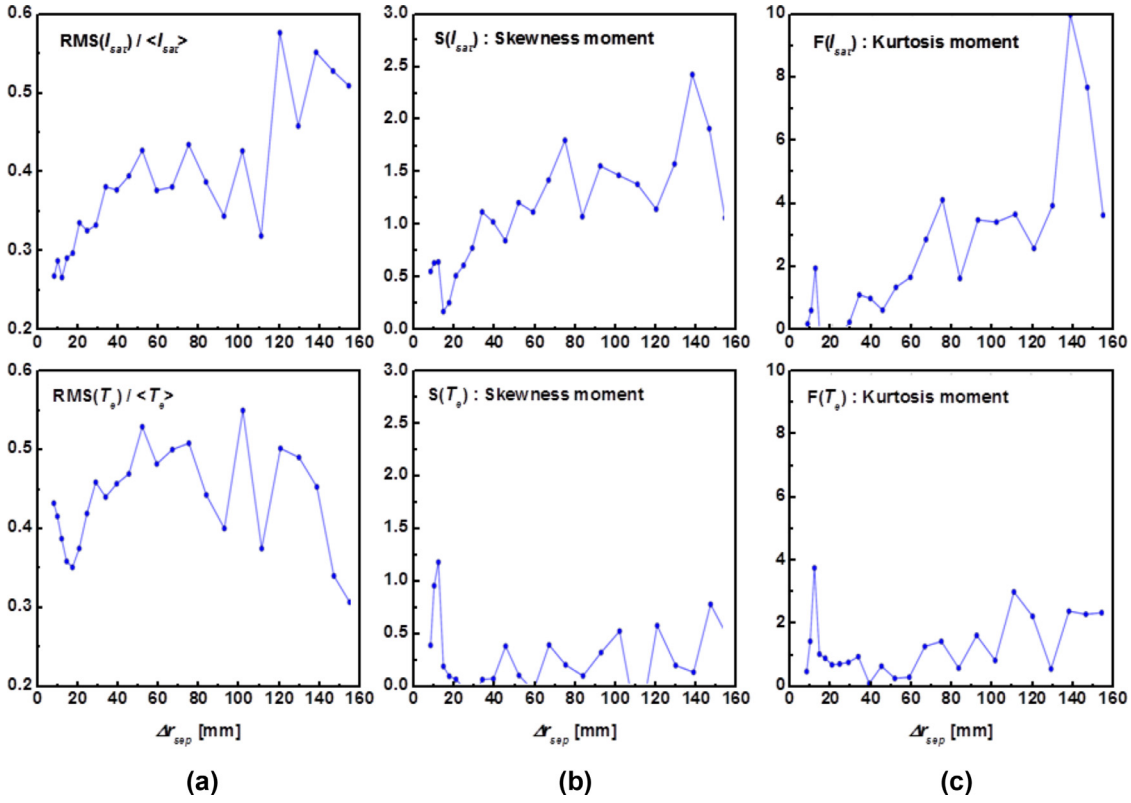

Fig. 9. Radial profiles of (a) the relative fluctuation levels, (b) the skewness moments and (c) the flatness moments for ion saturation current I_{sat} and electron temperature T_e obtained from the FRLPA measurement at the OMP.

behaviour of the fluctuations in T_e or I_{sat} in passing across the narrow and broad SOL regions.

Acknowledgements

This work was supported by Korea Ministry of Science, ITC and Future Planning under the KSTAR project contract and also partially supported by National Research Council of Science and Technology (NST) under the international collaboration & research in Asian counties. The views and opinions expressed here do not necessarily reflect those of the ITER Organization. ITER is the Nuclear Facility INB-174. The authors thank Mr. J.H. Jang and Prof. W.H. Choi in the Korea Advanced Institute of Science and Technology (KAIST) for providing the radiative power data. OEG and RK were supported with financial subvention from the Research Council of Norway under grant 240510/F20.

References

[1] M. Kocan, et al., Nucl. Fusion 55 (2015) 033019.
[2] P.C. Stangeby, et al., J. Nucl. Mater. 463 (2015) 389.
[3] J. Horacek, et al., J. Nucl. Mater. 463 (2015) 385.
[4] R. Dejarnac, et al., J. Nucl. Mater. 463 (2015) 381.
[5] F. Nespoli, et al., J. Nucl. Mater. 463 (2015) 393.
[6] J. Horacek, et al., Plasma Phys. Control. Fusion 58 (2016) 074005.
[7] J.G. Bak, et al., J. Nucl. Mater. 463 (2015) 424.
[8] J.G. Bak, et al., Contrib. Plasma Phys. 53 (2013) 69.
[9] D.C. Seo, et al., Improvement of the Lens system of IRTV and heat flux measurement on the inner wall limiter in KSTAR, in: the 21st Topical Conference on High-Temperature Plasma Diagnostics, Madison, Wisconsin, June 5-9, 2016.
[10] O.E. Garcia, et al., Nucl. Mater. Energy. (Accepted for publication, 12 November, 2016).
[11] H.S. Kim, et al., Fusion Eng. Des. 109-111 (2016) 809.
[12] C.S. Kang, et al., Rev. Sci. Instrum. 87 (2016) 083508.
[13] O.E Garcia, et al., Nucl. Fusion 47 (2007) 667.
[14] B. LaBombard, et al., Nucl. Fusion 45 (2005) 1658.
[15] D.L. Rudakov, et al., Nucl. Fusion 45 (2005) 1589.
[16] R.J. Goldston, J. Nucl. Mater. 463 (2015) 397.